

Optimization of a Novel Magneto-Rheological Device with Permanent Magnets

Mauro Tucci^{1, *}, Luca Sani¹, Vincenzo Di Dio²

Abstract—In this paper a novel evolutionary algorithm is used for the optimization of the performance of a magnetorheological (MR) device, capable to transmit torque between two shafts and powered by a system of Permanent Magnets (PMs). The stochastic, evolutionary, global optimization algorithm is based on a modified version of the self-organizing map. It uses a dedicated simplified analytical model of the device, developed in order to obtain a fast and accurate evaluation of the torque. Then, by means this model, the cost function to find the optimal parameters of the device is defined. Once the optimal parameters are identified, the performance of the proposed device is simulated by means of a FEM software. The results in terms of magnetic flux density inside the fluid, the transmissible torque and the actuation torque necessary to perform the device activation are discussed. Finally, a preliminary experimental validation of the proposed device is performed.

1. INTRODUCTION

Magneto-Rheological Fluids (MRFs) belong to the class of “smart fluid” and are a suspension of micrometer-sized ferromagnetic particles in a carrier fluid (synthetic oil or water). When subjected to an externally applied magnetic field the particles form columns and align themselves in the direction of the applied field. These columns act to resist shearing or the flow of the fluid, allowing a rapid transition from a liquid to a near-solid state. The apparent yield stress of the fluid is dependent on and increases with the intensity of the applied magnetic field [1, 2]. By removing the magnetic field, these fluids can return to their liquid state in less than 15–20 ms, with the phenomenon perfectly reversible [3]. MRFs exhibit such a behavior in three operational modes, namely shear, flow, and squeeze modes. In shear and squeeze modes, the fluid resists the motion of the plates perpendicular to or along the applied field, respectively; in flow mode, the flow of the fluid itself is resisted due to the particle columns formed. By using MRFs, an actuation system can be constructed such that the amount of torque/force it transmits can be controlled by varying the intensity of the applied field.

Many typical MRF-based devices have been developed in the past decades. The main applications are in dampers (used to absorb mechanical shocks and vibrations) or in finishing processes [4, 5]. Furthermore, several applications of MRF-based actuators in haptic and tactile feedback devices have been recently reported in the literature [6–12].

As for magnetorheological brakes or clutches, many solutions based on the shear mode have been developed in the past years [13–20]. In these devices, the use of MR fluids allows to obtain smooth and steady transmissible/braking torque, with many potential applications especially when simple structure, smooth, reliable and variable compliance are desirable characteristics (i.e., in automotive industry, robotics, and gym/fitness equipments). The majority of the currently available MR devices use conventional wired electromagnets to activate the fluid. Although they are characterized by a very

Received 18 September 2017, Accepted 13 November 2017, Scheduled 27 November 2017

* Corresponding author: Mauro Tucci (mauro.tucci@unipi.it).

¹ DESTEC, Department of Energy and Systems Engineering, University of Pisa, Italy. ² DEIM, Department of Energy, Engineering Information and Mathematical model, University of Palermo, Palermo, Italy.

simple control and actuation, some drawbacks have to be addressed. Firstly, the torque vs volume ratio is lower than the PMs based devices, since the permanent magnets are more effective in energizing the fluid. Then, in order to obtain a suitable level of magnetic field inside the fluid, a very thin MRF gap (< 0.5 mm) should be designed, increasing some manufacturing problems and affecting the performance of the fluid itself. Furthermore, the current in the electromagnets produces power losses which increase the temperature of the MRF, so reducing the transmissible/braking torque. Finally, in case of electric failure the fail-safe operation is not assured.

Fewer MR clutches/brakes are based on a combined permanent magnets/wired electromagnets system [21, 22, 24]. This hybrid solution uses a system of permanent magnets to produce the main magnetic field and conventional electromagnets, capable to develop a field in the opposite direction to one of the PMs, in order to control/modulate the magnetic field inside the MRF. Although these solutions allow obtaining higher torque with respect to the pure electromagnets-based device, the torques vs volume ratio and the complexity of the system are increased.

Finally, very few examples of fluid excitation based on a pure PMs system can be found in literature [15, 17–23, 25–28]. This solution has some advantages with respect to the conventional wired excitation system. Beside the reduction of power consumption, it allows obtaining better performance in terms of torque vs volume device ratio. Furthermore, due to high performance of the last generation of permanent magnets, a thick fluid gap of about 1.5 mm can be used. Then the PMs system does not produce power dissipation and temperature increase of the MRF and device. Finally, the use of permanent magnets could assure an intrinsic fail-safe operation in case of failure of the actuation control system. As for the main drawback, it should be noted that the use of rare-earth NdFeB permanent magnets surely increases the production costs with respect to the electromagnets-based devices.

In the present paper, a novel Magneto-Rheological device excited by permanent magnets is described and optimized. Although it could be used both as a clutch and as a brake, in the following sections the latter application is considered. The performance optimization of the device is obtained by means of a stochastic, evolutionary, global optimization algorithm, based on a modified version of the self-organizing map. For this purpose, a dedicated simplified analytical model, based on an equivalent magnetic network, has been developed in order to obtain a fast and accurate evaluation of the electromagnetic quantities. Then, the results in terms of magnetic flux density inside the fluid, transmissible torque and actuation torque necessary to perform the device activation have been discussed, also by comparison with the ones obtained by FEM software. Finally, a preliminary experimental validation of the proposed device has been performed.

2. THE MR FLUID

In this study, the magnetorheological fluid *MRF 140CG*, produced by Lord Corporation[®], Cary NC, USA [29], has been employed. The main magnetic and mechanical characteristics are synthesized by the $B - H$ curve and $\tau - H$ curve (Yield/Shear stress τ vs magnetic field H), shown in Figure 1.

As known, the operation of an MRF can be described by considering a sample of fluid located in a gap between two plates or two concentric cylinders. When subjected to an externally applied magnetic field, the micrometer-sized ferromagnetic particles in the fluid form columns and align themselves in the direction of the applied field. These columns act to resist shearing or the flow of the fluid, preventing

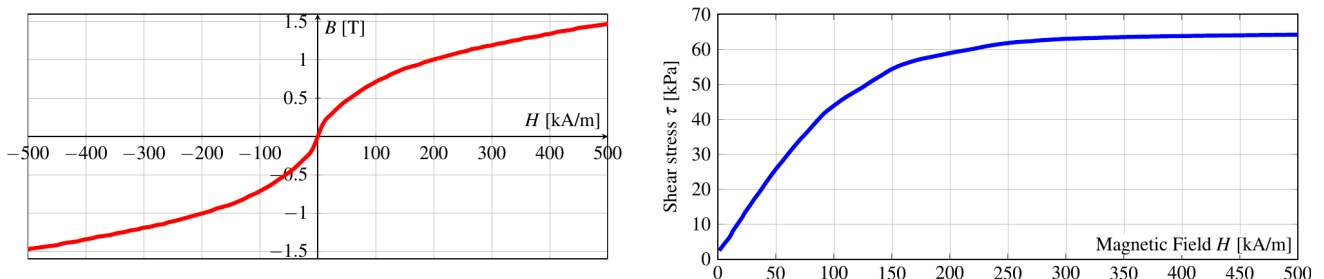


Figure 1. The $B - H$ curve and $\tau - H$ curve for a MRF140CG fluid.

the movement of the fluid particles themselves (transition from a liquid to a near-solid state). On the contrary, once the magnetic field has been removed, the ferromagnetic particles are randomly distributed in the volume, and the fluid is in a liquid state. This behavior can be described by the following equations, which represent the simplified model for these fluids:

$$\begin{cases} \tau = \tau_0(B_{\perp}) + \eta\dot{\lambda} & \text{if } \tau \geq \tau_0(B_{\perp}); \\ \dot{\lambda} = 0 & \text{if } \tau < \tau_0(B_{\perp}); \end{cases} \quad (1)$$

where $\tau_0(B_{\perp})$ is the yield/shear stress as a function of the magnetic induction orthogonal to the gap surfaces; $\eta = 0.28 \text{ Pa} \cdot \text{s}$ is the viscosity of the fluid at rest ($B = 0$); $\dot{\lambda} = r \cdot \frac{d\omega_r}{dr}$ is the fluid shear rate, with ω_r rotational speed in the fluid at radius r . From these equations it can be said that if an external action produces a shear stress $\tau \geq \tau_0(B_{\perp})$, the fluid shear rate $\dot{\lambda} \neq 0$ and the fluid begins its transition towards a liquid state; on the contrary, if $\tau < \tau_0(B_{\perp})$, the fluid shear rate $\dot{\lambda} = 0$ and the MRF has a semi-solid behavior.

In order to simplify the model, combining the $B-H$ curve and $\tau-H$ curve, the following relationship between yield/shear stress τ and magnetic induction B_{\perp} can be used [14, 30]:

$$\tau_0(B_{\perp}) = 66.73 \cdot B_{\perp}^4 - 222.40 \cdot B_{\perp}^3 + 200.07 \cdot B_{\perp}^2 + 17.27 \cdot B_{\perp} + 0.1817 \quad (2)$$

3. THE DEVICE

The basic configuration of the proposed MR device is shown in Figure 2. It is composed of two shafts (namely shaft#1 and shaft#2), magneto-rheological fluid, and fluid excitation system, which consists of four pie-shaped rare-earth NdFeB magnets ($B_r = 1.3 \text{ T}$; $H_c = 10.1 \cdot 10^5 \text{ A/m}$). They are alternately magnetized along the radial direction and are embedded in a chamber inside the shaft#1. Each of them occupies an angle of 45° along the circumferential direction, as shown in the figure. The shaft#1 is composed of four 90° -sections of ferromagnetic materials [31, 32]; two of these (opposite) sections are made of solid homogeneous material (AISI-1018), while in the other two opposite sections, a number of non-ferromagnetic plates (AISI-304) are inserted in order to better address the magnetic flux inside the MR fluid, avoiding the shunt of the flux lines as happens in the solid sectors. The shaft#2 is composed of solid ferromagnetic material (AISI-1018), whose radial thickness is chosen assuring that the magnetic induction is below the saturation level.

The proposed device operates as schematically shown in Figures 2(b) and (c). Let's assume that initially the excitation system (i.e., the PMs) is in the OFF state (see Figure 2(b)); since the magnetic flux lines close themselves in the two solid ferromagnetic sectors of the shaft#1 (which act as a shunt for the flux just below the MRF), the magnetic field does not pass through the fluid. In this condition, the shaft#2 rotates at a given speed while the shaft#1 is at rest. Once the decision to brake the shaft#2 has been taken, the excitation system must be rotated inside the housing chamber along its circumferential direction (indifferently in clockwise or counter clockwise), with respect to the shaft#1. During the rotation of the PMs, the presence of non-ferromagnetic plates in the two opposite sections of the shaft#1 progressively forces the magnetic field to cross the fluid and to close its flux lines, following the path of least reluctance through the shaft#2. The highest values of the field inside the MRF and, consequently, of the braking torque are obtained when the excitation system has been rotated by an angle of 90° , working in the ON state (see Figure 2(c)).

However, considering that the radial thickness of the permanent magnets and of the shaft#1 as well as the circumferential dimensions of the non-ferromagnetic plates greatly affect the value of the magnetic induction in the fluid both in the OFF and ON state, a multiobjective optimization procedure (see Section 5) has been used to identify these parameters. Then, in order to obtain a fast and accurate evaluation of the magnetic and mechanical quantities to be optimized [33–36], a simplified model of the device based on equivalent magnetic network has been developed.

4. THE ANALYTICAL MODEL

The analysis of the electromagnetic behavior of the proposed device requires a complex 3D FEM model. However, by setting some simplifying assumptions and taking into account the approximation errors,

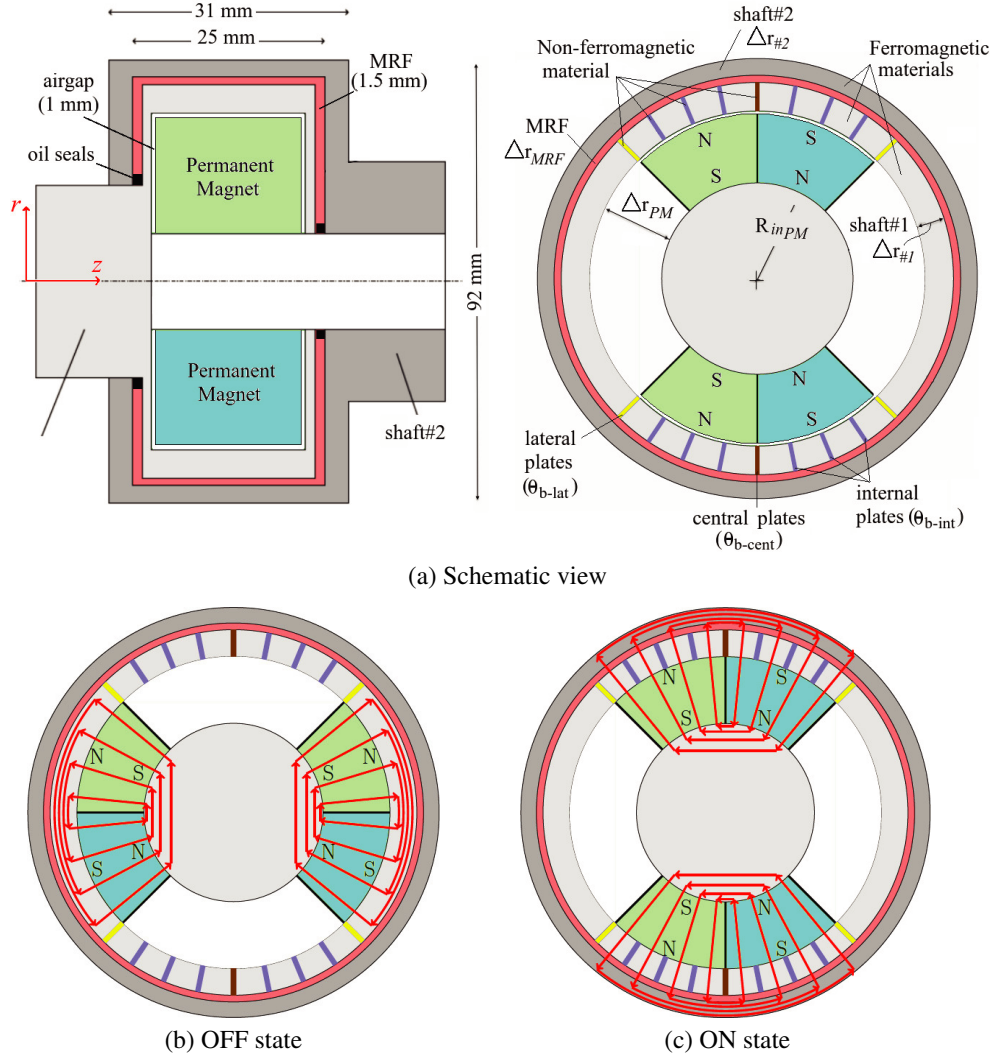


Figure 2. Schematic view of the proposed device with the main dimensions and the operation principle.

the magnetic field can be obtained by using a magnetic circuit of lumped reluctances. It is assumed that all magnetic materials are linear and that the magnetic field do not vary along the z -direction (2D model). Furthermore, this 2D analysis neglects the contribution to the braking torque of the MRF that fills the gaps at the two bases of the cylindrical structure.

In order to build the magnetic circuit, the cross-sectional area of the device has been subdivided in a number of n_r and n_θ points respectively along the radial and circumferential directions. Four neighboring nodes constitute the vertex of an elementary area (or cell). Then, the four vertexes of each cell have been connected along the edges by four reluctances. Figure 3 shows the equivalent magnetic network, with reluctances and magneto-motive force generators, overlapping the device geometry when the PMs are in the ON state (for the sake of readability, all the radial dimensions have been enlarged).

The reluctances $\mathfrak{R}_{\gamma,\gamma} |_{\gamma=1,2,\dots,n_r}$, which connect two nodes having the same radius, are able to take into account the magnetic flux along the circumferential direction (“tangential flux”); on the contrary, reluctances $\mathfrak{R}_{\gamma-1,\gamma} |_{\gamma=1,2,\dots,n_r}$ between two nodes, characterized by the same angle, are able to consider the magnetic flux along the radial direction (“radial flux”).

As for the MRF and the external part of the shaft#2, both the reluctances $\mathfrak{R}_{\gamma,\gamma}$ and $\mathfrak{R}_{\gamma-1,\gamma}$ do not vary along the circumferential direction. On the contrary, the reluctances $\mathfrak{R}_{\gamma,\gamma}$ in the inner part of the shaft#1 depend on the circumferential direction. In particular, since from $+45^\circ < \theta < +135^\circ$ and

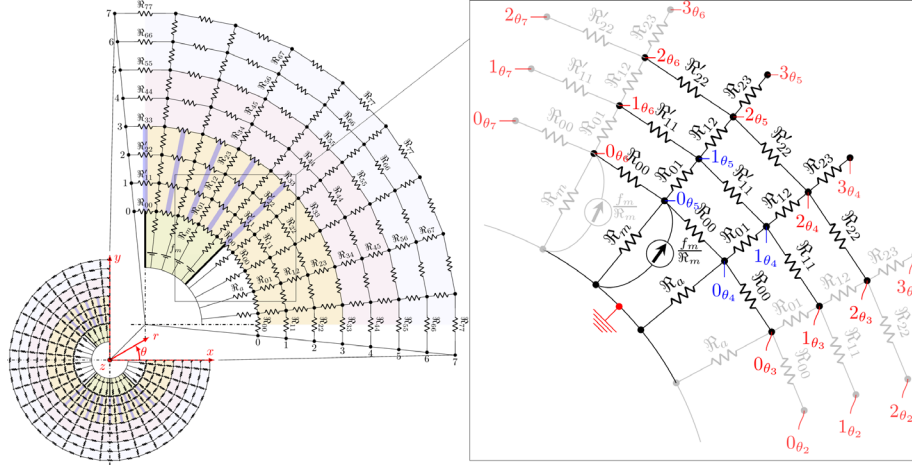


Figure 3. Schematic view of the equivalent magnetic network of the device in the ON state.

$+225^\circ < \theta < +315^\circ$ some non-ferromagnetic plates are inserted, the relative reluctances are different from that in the ranges from $+315^\circ < \theta < +45^\circ$ and $+135^\circ < \theta < +225^\circ$. Furthermore, the reluctances $\mathfrak{R}_{0,0}$ take into account the 1 mm-thick airgap between the excitation system and the shaft#1, which needs to allow the rotation of the magnets in order to activate/dis-activate the brake. Finally, considering the relative magnetic permeability of the PMs ($\mu_{r_{PM}} \simeq 1$), we can assume that the reluctances of the free space adjacent the magnets is equal to the reluctances of the PMs: $\mathfrak{R}_a \simeq \mathfrak{R}_m$.

Taking into account the dimensions of the devices and the magnetic characteristics of the materials, the following values for the reluctances can be calculated:

$$\mathfrak{R}_m = \frac{\Delta r_{PM}}{\mu_0 \mu_{r_{PM}} \bar{S}_m}, \quad \mathfrak{R}_{\gamma-1,\gamma}^{(x)} = \frac{\Delta r^{(x)}}{\mu_0 \mu_{r_{fe}} \bar{S}_{r^{(x)}}}, \quad \mathfrak{R}_{\gamma,\gamma}^{(x)} = \frac{\Delta \theta^{(x)}}{\mu_0 \mu_{r_{fe}} \bar{S}_{\theta^{(x)}}}, \quad \mathfrak{R}_{\gamma,\gamma}^{(x')} \simeq \mathfrak{R}_{\gamma,\gamma}^{(x)} + \frac{\Delta \theta^{(b)}}{\mu_0 \bar{S}_{\theta^{(x)}}},$$

where the superscript/subscript x is used to identify the different materials (inner/outer iron, MRF, etc.), while the subscript γ refers to the nodes of the discretization. The other main parameters are listed in Table 1.

Table 1. Description of the parameters for the calculation of the magnetic equivalent network

n_{rx}	number of points along the radial direction for the different materials (x);
n_θ	number of points along the circumferential direction;
ℓ_z	cell thickness along the z -direction;
$\Delta r_{PM} = (r_{out_{PM}} - r_{in_{PM}})$	length of the PM along the radial direction;
$\Delta r^{(x)} = \left(\frac{r_{out_x} - r_{in_x}}{n_{rx} - 1} \right)$	length of the cell along the radial direction for each material;
$\Delta \theta^{(x)} = \left[r_{in_x} + (2\gamma - 1) \frac{\Delta r^{(x)}}{2} \right] \cdot \frac{2\pi}{n_\theta - 1} \Big _{\gamma=1,2,\dots,n_{rx}-1}$	length of the cell along the circumferential direction for each material (excluding non-ferromagnetic plates);
$\Delta \theta^{(b)} = \left[r_{in_x} + (2\gamma - 1) \frac{\Delta r^{(x)}}{2} \right] \cdot \theta_b \Big _{\gamma=1,2,\dots,n_{rx}-1}$	length of non-ferromagnetic plates of angle θ_b along the circumferential direction;
$\bar{S}_m = \left(r_{in_{PM}} + \frac{\Delta r_{PM}}{2} \right) \cdot \frac{2\pi}{n_\theta - 1} \cdot \ell_z$	PM average cross-sectional area along the radial direction;
$\bar{S}_{r^{(x)}} = \Delta \theta^{(x)} \cdot \ell_z$	cell average cross-sectional area along the radial direction;
$\bar{S}_{\theta^{(x)}} = \Delta r^{(x)} \cdot \ell_z$	cell average cross-sectional area along the circumferential direction;

As for the magnetic source, since the PMs are magnetized along the radial direction, the magnetomotive force (mmf) can be obtained as $f_m = \pm |H_c| \cdot \Delta r_{PM}$, where $|H_c| = 10.2 \cdot 10^5$ A/m is the coercivity of the magnet, and the “ \pm ” sign accounts for the reversed polarity of the PMs.

Once the values of the elements of the equivalent magnetic network have been calculated, the Nodal Analysis Method for the electrical network is used to solve the problem [37],[38]. As an example of the set of equations obtained by the model, in the right side of Figure 3 a portion of the equivalent magnetic network is shown. For the sake of simplicity, the real mmf generators (simulating the PMs) are replaced by their Norton equivalent circuits, each of them composed of a magnetic flux generator ($\varphi_m^* = f_m/\mathfrak{R}_m$) in shunt with the reluctance \mathfrak{R}_m .

The equations, written respectively at the nodes 0_{θ_4} , 1_{θ_4} , 0_{θ_5} , 1_{θ_5} , are:

$$\left\{ \begin{array}{l} 0_{\theta_4} \Rightarrow 0 = \mathcal{F}_0^{(\theta_4)} \left(\frac{1}{\mathfrak{R}_a} + \frac{1}{\mathfrak{R}_{00}} + \frac{1}{\mathfrak{R}_{01}} + \frac{1}{\mathfrak{R}_{00}} \right) - \left(\frac{\mathcal{F}_0^{(\theta_3)}}{\mathfrak{R}_{00}} \right) - \left(\frac{\mathcal{F}_1^{(\theta_4)}}{\mathfrak{R}_{01}} \right) - \left(\frac{\mathcal{F}_0^{(\theta_5)}}{\mathfrak{R}_{00}} \right); \\ 1_{\theta_4} \Rightarrow 0 = \mathcal{F}_1^{(\theta_4)} \left(\frac{1}{\mathfrak{R}_{01}} + \frac{1}{\mathfrak{R}_{11}} + \frac{1}{\mathfrak{R}_{12}} + \frac{1}{\mathfrak{R}'_{11}} \right) - \left(\frac{\mathcal{F}_0^{(\theta_4)}}{\mathfrak{R}_{01}} \right) - \left(\frac{\mathcal{F}_1^{(\theta_3)}}{\mathfrak{R}_{11}} \right) - \left(\frac{\mathcal{F}_2^{(\theta_4)}}{\mathfrak{R}_{12}} \right) - \left(\frac{\mathcal{F}_1^{(\theta_5)}}{\mathfrak{R}'_{11}} \right); \\ 0_{\theta_5} \Rightarrow + \frac{f_m}{\mathfrak{R}_m} = \mathcal{F}_0^{(\theta_5)} \left(\frac{1}{\mathfrak{R}_m} + \frac{1}{\mathfrak{R}_{00}} + \frac{1}{\mathfrak{R}_{01}} + \frac{1}{\mathfrak{R}_{00}} \right) - \left(\frac{\mathcal{F}_0^{(\theta_4)}}{\mathfrak{R}_{00}} \right) - \left(\frac{\mathcal{F}_1^{(\theta_5)}}{\mathfrak{R}_{01}} \right) - \left(\frac{\mathcal{F}_0^{(\theta_6)}}{\mathfrak{R}_{00}} \right); \\ 1_{\theta_5} \Rightarrow 0 = \mathcal{F}_1^{(\theta_5)} \left(\frac{1}{\mathfrak{R}_{01}} + \frac{1}{\mathfrak{R}'_{11}} + \frac{1}{\mathfrak{R}_{12}} + \frac{1}{\mathfrak{R}'_{11}} \right) - \left(\frac{\mathcal{F}_0^{(\theta_5)}}{\mathfrak{R}_{01}} \right) - \left(\frac{\mathcal{F}_1^{(\theta_4)}}{\mathfrak{R}'_{11}} \right) - \left(\frac{\mathcal{F}_2^{(\theta_5)}}{\mathfrak{R}_{12}} \right) - \left(\frac{\mathcal{F}_1^{(\theta_6)}}{\mathfrak{R}'_{11}} \right); \end{array} \right.$$

where $\mathcal{F}_j^{(\theta_k)}$ is the unknown magnetomotive force of the j -node along the radial direction at the θ_k angle along the circumferential direction.

This procedure has been extended to all the nodes of the network, resulting in a set of simultaneous algebraic equations with constant coefficients. Then, this equations set can be arranged in a $[(n_r - 1) \cdot n_\theta] \times [(n_r - 1) \cdot n_\theta]$ matrix form and solved by means of conventional mathematical method:

$$\left| \begin{array}{c} 0 \\ 0 \\ \vdots \\ + \frac{f_m}{\mathfrak{R}_m} \\ \vdots \\ - \frac{f_m}{\mathfrak{R}_m} \\ 0 \end{array} \right| = \left\| \begin{array}{cccc} \mathcal{P}_{11} & \mathcal{P}_{12} & \cdots & \mathcal{P}_{1(n_r-1) \cdot n_\theta} \\ \mathcal{P}_{21} & \mathcal{P}_{22} & \cdots & \mathcal{P}_{2(n_r-1) \cdot n_\theta} \\ \vdots & \vdots & \ddots & \vdots \\ \vdots & \vdots & \ddots & \vdots \\ \vdots & \vdots & \ddots & \vdots \\ \mathcal{P}_{(n_r-1) \cdot n_\theta 1} & \cdots & \cdots & \mathcal{P}_{(n_r-1) \cdot n_\theta (n_r-1) \cdot n_\theta} \end{array} \right\| \cdot \left\| \begin{array}{c} \mathcal{F}_0^{(\theta_1)} \\ \mathcal{F}_1^{(\theta_1)} \\ \vdots \\ \vdots \\ \vdots \\ \mathcal{F}_{n_r-1}^{(\theta_{n_\theta})} \end{array} \right\| \Rightarrow |\varphi| = \|\mathcal{P}\| \cdot |\mathcal{F}| \Rightarrow |\mathcal{F}| = \|\mathcal{P}\|^{-1} \cdot |\varphi|$$

where \mathcal{P}_{ij} terms are constant coefficients. Once the $(n_r - 1) \cdot n_\theta$ mmf $\mathcal{F}_j^{(\theta_k)}$ are known at all the nodes, the magnetic flux density in each branch of the network (that is in each material of the device) can be calculated. In particular, since the braking torque depends on the radial component of the magnetic induction inside the MR fluid, for each circumferential coordinate, this quantity can be calculated as:

$$B_\perp = \frac{\mathcal{F}_j^{(\theta_k)} - \mathcal{F}_{j-1}^{(\theta_k)}}{\mathfrak{R}_{j-1,j}} \cdot \frac{1}{\bar{S}_{MRF}},$$

where $\mathfrak{R}_{j-1,j}$ is the reluctance crossing the circumference trough the center of the MRF; $\mathcal{F}_j^{(\theta_k)} - \mathcal{F}_{j-1}^{(\theta_k)}$ is the difference of the mmf across the reluctance; $\bar{S}_{MRF} = \left[\frac{r_{inMRF} + r_{outMRF}}{2} \right] \cdot \frac{2\pi}{n_\theta - 1} \cdot \ell_z$ is the average cross-sectional area along the radial direction of a $\frac{2\pi}{n_\theta - 1}$ portion of the fluid. However, in the case of an even number of reluctances along the radial direction inside the MRF, B_\perp can be obtained as the

average value between the magnetic induction calculated using the reluctances which have the common node on the circumference through the center of the fluid.

As for the braking torque, each cell of MR fluid produces the following contribution:

$$\Delta T_b = \tau \cdot \left[\frac{r_{in_{MRF}} + r_{out_{MRF}}}{2} \right]^2 \cdot \Delta\theta \cdot \ell_z = \left[\tau_0 (B_{\perp}) + \eta \dot{\lambda} \right] \cdot \left[\frac{r_{in_{MRF}} + r_{out_{MRF}}}{2} \right]^2 \cdot \Delta\theta \cdot \ell_z \quad (3)$$

then, taking into account the number of cells along the circumferential direction, the total torque developed by the proposed brake is:

$$T_b = \sum_{sup} \Delta T_b = \sum_{sup} \left[\tau_0 (B_{\perp}) + \eta \dot{\lambda} \right] \cdot \left[\frac{r_{in_{MRF}} + r_{out_{MRF}}}{2} \right]^2 \cdot \Delta\theta \cdot \ell_z \quad (4)$$

where the shear rate in the center of the fluid is $\dot{\lambda} = r \cdot \frac{d\omega_r}{dr} \simeq \frac{\left[\frac{r_{in_{MRF}} + r_{out_{MRF}}}{2} \right] \cdot \Delta\Omega}{r_{out_{MRF}} - r_{in_{MRF}}}$, and $\Delta\Omega$ is the relative angular speed between the two shafts.

4.1. Preliminary Model Validation by FEM

In order to perform a preliminary validation of the analytical model, some FEM simulations have been carried out by means of the code EFFE [39]. The results of the analytical model have been obtained by using 8 and 33 points respectively along the radial and circumferential directions. Furthermore, 9 non-ferromagnetic plates with the same circumferential dimension $\theta_b = 0.05 \text{ rad} (\simeq 3^\circ)$ have been considered for each of the two (opposite) sections of the shaft#1. Figure 4 shows the comparison between the analytical and numerical radial component of the magnetic induction B_r on the circumference passing through the center of the MR fluid in the ON and OFF state. The agreement between the two models is satisfactory and confirms the goodness of the developed analytical model. Furthermore, the results show that when the excitation system is in the ON state, the values of B_r are high enough to produce the braking torque. On the contrary, when the PMs are in the OFF condition, the maximum values of the magnetic induction in the fluid are very low ($\simeq 60 \text{ mT}$), resulting in a small torque.

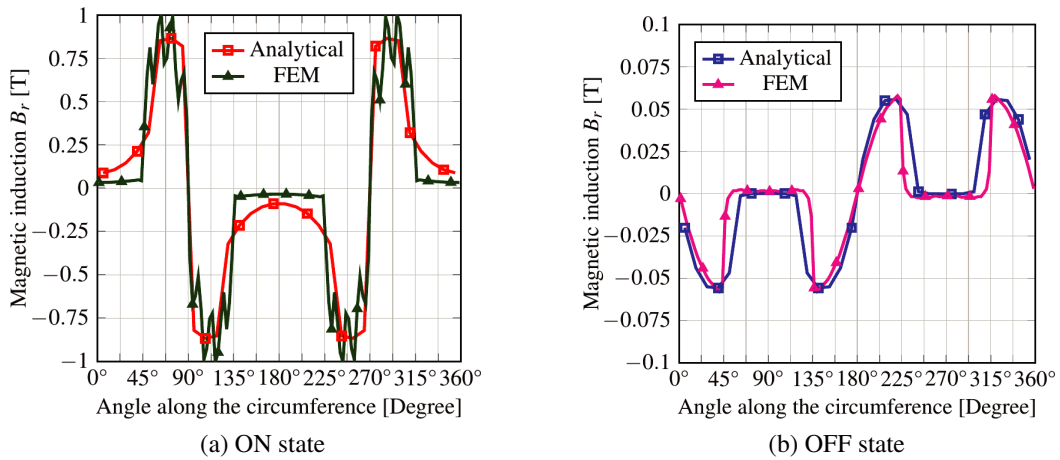


Figure 4. Radial component of the magnetic induction in the MR fluid, in the ON and OFF state.

5. THE OPTIMIZATION ALGORITHM

Given the outer diameter of the device ($\phi_{out} = 92 \text{ mm}$) and its axial length ($\ell_z = 31 \text{ mm}$), the thickness of the gap filled by the MRF ($\Delta r_{MRF} = 1.5 \text{ mm}$), and the airgap between the PMs and the housing chamber ($g = 1 \text{ mm}$). The main parameters which affect the performance of the proposed brake are: 1) the radial thickness of the permanent magnets: Δr_{PM} ; 2) the radial thickness of shaft#1: $\Delta r_{\#1}$; 3)

the circumferential dimension of the non-ferromagnetic plates. However, once the inner radius of the PMs ($R_{inPM} = 10$ mm) and the radial thickness of shaft#2 ($\Delta r_{\#2} = 7.5$ mm) are chosen in order to not overcome the saturation level of the iron, parameters 1) and 2) are correlated in such a way that $2 \cdot (R_{inPM} + \Delta r_{PM} + g + \Delta r_{\#1} + \Delta r_{MRF} + \Delta r_{\#2}) = \phi_{out}$.

Furthermore, by analyzing the paths of the magnetic flux in the system both in the ON and OFF states, three different kinds of non-ferromagnetic plates can be identified (see Figure 2): a) the (four) “lateral plates”, positioned in correspondence of the borders of the PMs (at the angles 45° , 135° , 225° , and 315°); b) the (two) “central plates”, positioned at the angles 90° , and 270° ; and c) the (twelve) “internal plates”, equally distributed in the space between the lateral and central plates. Also the number of these latter non-ferromagnetic plates is chosen taking into account the saturation level of the iron between two consecutive plates.

On the basis of these considerations and by using the analytical model developed and validated in the previous section, the problem consists in optimizing a number of objective functions, $F_i(\mathbf{x})$, $i = 1 \dots N_f$, where $\{F_i : \Omega \subseteq \mathbb{R}^n \rightarrow \mathbb{R}\}$, $\mathbf{x} \in \Omega$, and Ω is the domain of the search. Beside the geometrical constraints, the procedure assures also that the device works below the saturation level of the ferromagnetic material.

In particular, the two objective functions are:

- (i) $F_1(\mathbf{x})$: the braking torque T_{ON} (eq. 4) in the ON state (to be maximized, so we minimize $-F_1(\mathbf{x})$);
- (ii) $F_2(\mathbf{x})$: the braking torque T_{OFF} (eq. 4) in the OFF state (to be minimized).

As for the parameters vector \mathbf{x} , it consists in four geometrical variables:

- Δr_{PM} : radial thickness of the PMs;
- $\theta_{(b-lat)}$: circumferential dimension of the lateral non-ferromagnetic plates;
- $\theta_{(b-cent)}$: circumferential dimension of the central non-ferromagnetic plates;
- $\theta_{(b-int)}$: circumferential dimension of the interior non-ferromagnetic plates.

Finally, the problem constraints are:

- bounds on the geometrical parameters, given as maximum and minimum allowed values:
 - a) $10 \text{ mm} \leq \Delta r_{PM} \leq 20 \text{ mm}$;
 - b) $0.5^\circ \leq [\theta_{(b-lat)}; \theta_{(b-cent)}; \theta_{(b-int)}] \leq 11^\circ$;
- maximum absolute value of the magnetic induction in the iron is set to 2 Tesla.

Since the objective functions have a large number of local minima and a optimum Pareto front is searched, an evolutionary optimization algorithm [40] is used in this work. It is based on the self-organizing maps (SOM), which are popular neural networks for unsupervised learning, clustering and data visualization. The SOM neural networks in general have a strong exploratory power, and the final centroids tend to be disposed in a predefined topological order. In the proposed strategy, each cell of the SOM contains a centroid (or an individual) that searches for the Pareto optimal solutions. The global task is to track the Pareto optimal front, which is approximated by the set of non-dominated solutions found by all centroids in all generations. The movement of centroids is obtained using a discrete-time dynamical filter, and the choice of this filter is flexible. The resulting method is an heuristic optimization algorithm that uses some evolutionary computation mechanisms such as selection and mutation (perturbation). The algorithm tries to take advantage of the exploratory power of the SOMs: the collaboration between neighboring centroids enhances exploitation, whereas centroids that are far from each other will explore different areas of the search space, improving exploration and preserving diversification. Also, a complete constraints handling procedure is used. The optimization algorithm was proven to be tightly competitive with other state of the art evolutionary optimization algorithms such as genetic algorithms and particle swarm optimization algorithms. In particular, the SOM-based algorithm allows performing tens of thousands of function evaluations in few minutes, obtaining a very fast and satisfactory optimal design with respect to several variables in multi-objective optimization.

These features can be effectively used also when complex problems should be analyzed. In this case, a simplified analytical model can be developed and preliminarily optimized by using the proposed algorithms. Then this basic optimal solution can be further improved by using a FEM-based

optimization tool, so saving a significant amount of simulation time. On the contrary, if one uses a FEM optimization procedure from scratch, the computation times would be extremely long.

In this work, the number of individuals of the population is set to 100, using a 10×10 grid of the SOM. The algorithm reached the final results performing 45000 evaluations in about 20 minutes on a 12-core, 32Gb RAM, 3.6 GHz PC. Figure 5 shows the Pareto front obtained at the end of the optimization procedure, while in Table 2 the values of the optimized parameters and relative braking torques (in the ON and OFF state) are reported.

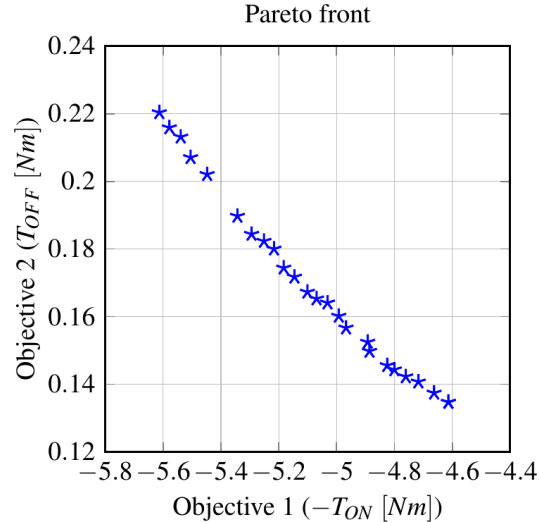


Figure 5. The Pareto front.

6. RESULTS AND PRELIMINARY EXPERIMENTAL TESTS

Although several criteria can be used to choose a solution between those shown in Table 2 (e.g., the configuration which maximize the ratio $\frac{T_{ON}}{T_{OFF}}$, or the one that minimize the PMs volume), in the following the combination of parameters which maximize the braking torque in the ON state has been considered. In particular, taking into account the accuracy of the numerical results and some criteria related to an easy manufacturing and assembly, the values of the parameters reported in the 2nd row of Table 2 have been selected as the preferred solution and approximated as follows:

- $\Delta r_{PM} = 14$ mm; $\Delta r_{\#1} = 12$ mm;
- $\theta_{(b-lat)} = 0.175$ rad ($\simeq 10^\circ$); $\theta_{(b-cent)} = 0.175$ rad ($\simeq 10^\circ$); $\theta_{(b-int)} = 0.09$ rad ($\simeq 5^\circ$);

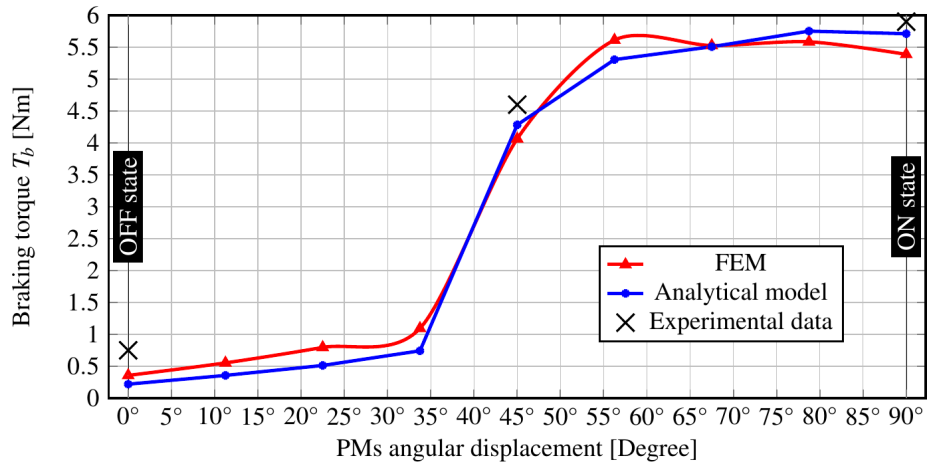
Then, the braking torque developed by the proposed device has been calculated. Figure 6 shows its value as a function of the position of the excitation system along the circumferential direction. When the PMs are in the ON state (angular displacement = 0°), the braking torque is about 5.6 Nm, while in the OFF state (angular displacement = 90°) the torque is about 0.23 Nm. This latter value is mainly due to the fluid natural viscosity. Anyhow, the ratio between the maximum and minimum torques, which is between the torques in the ON and OFF states, for the proposed brake is about 24, an excellent value in this kind of device.

In the same figure, some very preliminary experimental data are shown. They have been obtained by using a very simple test bench (see Figure 7). The braking torque has been measured respectively when the excitation system was in the OFF state, in the intermediate position (45°) and in the ON state. However, taking into account that the simulation results neglect the contribution to the braking torque of the MRF which fills the gaps at the two bases of the cylindrical structure, the simulated and measured values of the torque match quite well.

In order to compare the performance of the proposed device with respect to other similar MRF-based clutches/brakes described in literature, some data are reported in Table 3. In particular, in the

Table 2. The optimized parameters (arranged in descending order w.r.t. T_{ON}).

Δr_{PM} [mm]	$\Delta r_{\#1}$ [mm]	$\theta_{(b-int)}$ [rad]	$\theta_{(b-lat)}$ [rad]	$\theta_{(b-cent)}$ [rad]	T_{ON} [Nm]	T_{OFF} [Nm]	T_{ON}/T_{OFF}
14.2	11.8	0.1030	0.165	0.171	5.61	0.220	25.5
14.0	12.0	0.0974	0.170	0.170	5.58	0.216	25.8
13.9	12.1	0.1000	0.168	0.150	5.54	0.213	26.0
13.7	12.3	0.1030	0.165	0.171	5.50	0.207	26.6
13.5	12.5	0.0931	0.175	0.152	5.45	0.202	27.0
13.0	13.0	0.0989	0.167	0.161	5.34	0.190	28.2
12.7	13.3	0.0955	0.165	0.169	5.29	0.184	28.7
12.7	13.3	0.0782	0.176	0.147	5.25	0.182	28.8
12.6	13.4	0.0822	0.176	0.140	5.22	0.180	29.0
12.3	13.7	0.0895	0.173	0.158	5.18	0.174	29.7
12.2	13.8	0.0874	0.180	0.154	5.15	0.172	30.0
11.9	14.1	0.0940	0.172	0.156	5.10	0.167	30.5
11.8	14.2	0.0832	0.172	0.150	5.07	0.165	30.7
11.8	14.2	0.0815	0.172	0.136	5.03	0.164	30.7
11.6	14.4	0.0755	0.180	0.143	4.99	0.160	31.2
11.4	14.6	0.0844	0.174	0.152	4.97	0.157	31.7
11.1	14.9	0.0792	0.177	0.140	4.89	0.152	32.1
11.0	15.0	0.0978	0.176	0.161	4.89	0.150	32.6
10.7	15.3	0.0806	0.167	0.157	4.83	0.146	33.2
10.6	15.4	0.0884	0.176	0.151	4.80	0.144	33.3
10.5	15.5	0.0880	0.175	0.144	4.76	0.142	33.5
10.4	15.6	0.0896	0.176	0.133	4.72	0.141	33.5
10.2	15.8	0.0765	0.182	0.135	4.66	0.137	33.9
10.0	16.0	0.0745	0.184	0.132	4.61	0.135	34.2

**Figure 6.** The braking torque as a function of the angular position of the PMs.

proposed device, the excitation system needs to be powered just to be moved from the OFF to the ON state (and vice versa). Once the PMs have reached the (OFF or ON) position, the power is no longer necessary to keep the system in that position. The value of the maximum mechanical power required to rotate the PMs by an angle of 90° has been estimated by assuming that this movement can be performed in about 250 ms. This value considers only the magnetic torque (see Figure 8) and neglects the parasitic torque due for example to the bearings friction.

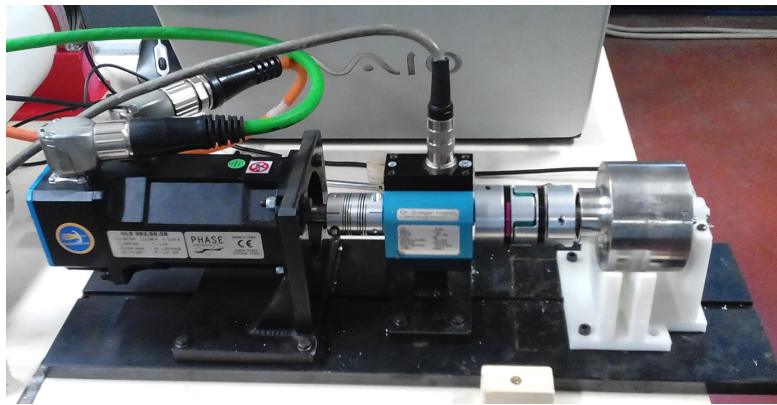


Figure 7. The test bench.

Table 3. Comparison between the proposed device and other similar MRF-based clutches/brakes.

	Unit	Proposed device	Lord Corp [29] RD-2068-10	Jie Wu et al. [14]	Bucchi et al. [17]
Max Torque (ON state)	Nm	5.8*	4	38	3.2
Min Torque (OFF state)	Nm	0.6*	0.4	2	0.5
Torque _{ON} /Torque _{OFF}	-	≈ 10	10	19	6.4
Axial length	mm	31	58	75	40
Diameter	mm	92	90	150	65
Volume	cm ³	206	≈ 370	1325	133
Max Torque/Volume	kN/m ²	28	11	28	24
Power	W	1.25**	15	17	—

*experimental values; **max mechanical power required to rotate the PMs by 90° in 0.25 s.

7. THE BRAKE ACTUATION

In order to activate the brake, the excitation system (that is the PMs) must be rotated along its circumferential direction (indifferently in clockwise or counter clockwise) by an angle of 90° with respect to the housing chamber. During the rotation, the PMs feel a magnetic torque that hinders their motion from the OFF to the ON state and vice-versa. This “activation” torque is due to the natural magnetic interaction between magnets and ferromagnetic materials which constitute the four sectors of the shaft#1. By using the FE model, the activation magnetic torque profile as a function of the PMs angular displacement has been obtained. As shown in Figure 8, the maximum value occurs when the permanent magnets system passes through the midway between the ON and OFF state.

As for the brake control strategy, a preloaded torsional spring can be used to overcome the magnetic torque and to rotate the PMs from OFF to ON state [41]. Then, an auxiliary mechanism (not shown in figure) can be exploited to move the permanent magnets from the ON to the OFF state.

Anyhow, the power required to activate/deactivate the proposed brake is a very low fraction of the braking power.

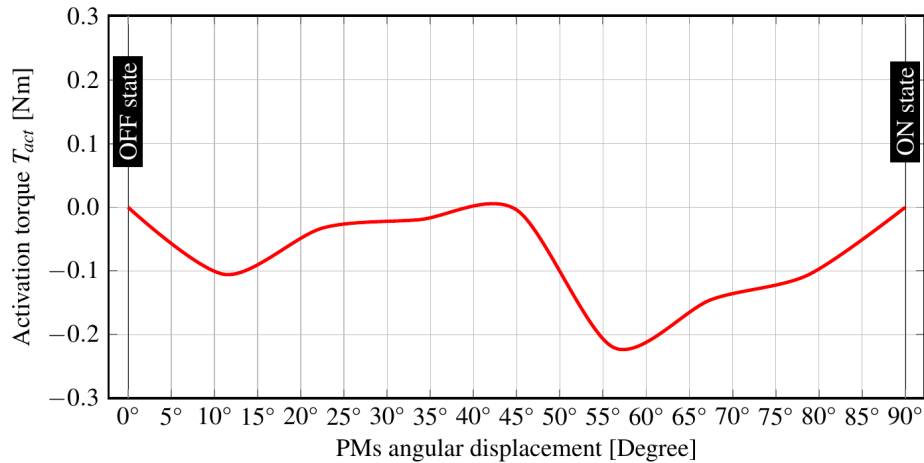


Figure 8. The activation torque as a function of the angular position of the PMs.

8. CONCLUSIONS

The authors have presented a magneto-rheological device excited by a system of permanent magnets. The device optimization has been obtained by using an evolutionary optimization algorithm, based on the self-organizing maps (SOM). Once the values of the optimized parameters have been obtained, the braking torque is calculated in the ON state ($\simeq 5.6$ Nm) and OFF state ($\simeq 0.23$ Nm), with a ratio of about 24, an excellent value in this kind of device. Finally, the performance under different operating conditions has been verified by means of a FE model and some preliminary experimental data.

REFERENCES

1. Carlson, J. D., D. N. Catanzarite, and K. A. St Clair, "Commercial magneto-rheological fluid device," *Proceedings 5th Int. Conf. on ER Fluids, MR Suspensions and Associated Technology*, W. Bullough (ed.), 20–28, World Scientific, Singapore, 1996.
2. Carlson, J. D., "The promise of controllable fluids," *Proc. of Actuator 94 (H. Borgmann and K. Lenz, Eds.)*, AXON Technologies Consult GmbH, 266–270, 1994.
3. Kordonsky, W. I., "Elements and devices based on magnetorheological effect," *J. Intell. Mater. Syst. Struct.*, Vol. 4, No. 1, 65–69, 1993.
4. Shorey, A. and M. DeMarco, "Application of magneto-rheological finishing (MRF) to the figuring of adaptive optics systems," *Adaptive Optics: Methods, Analysis and Applications*, Charlotte, North Carolina, June 6, 2005.
5. Lee, S. O., K. I. Jang, B. K. Min, S. J. Lee, and J. W. Seok, "A study on tribological properties of magneto-rheological fluid (MRF) in polishing process," *Proceedings of the KSPE Spring Conference*, Vol. 40, 20–33, 2006.
6. Rossa, C., J. Lozada, and A. Micaelli, "Interaction Power Flow Based Control of a 1-DOF Hybrid Haptic Interface," *Proceedings of International Conference, EuroHaptics 2012*, Tampere, Finland, June 13–15, 2012.
7. Bicchi, A., M. Raugi, R. Rizzo, and N. Sgambelluri, "Analysis and design of an electromagnetic system for the characterization of magneto-rheological fluids for haptic interfaces," *IEEE Trans on Mag.*, Vol. 41, No. 5, 1876–1879, May 2005.
8. Scilingo, E. P., R. Rizzo, N. Sgambelluri, M. Raugi, and A. Bicchi, "Electromagnetic modeling and design of haptic interface prototypes based on magnetorheological fluids," *IEEE Trans on Mag.*, Vol. 43, No. 9, September 2007.
9. Rizzo, R., "A permanent magnets exciter for MRF-based haptic interfaces," *IEEE Trans on Mag.*, Vol. 49, No. 4, 1390, 1401, April 2013.

10. Raugi, M., N. Sgambelluri, E. P. Scilingo, A. Bicchi, and R. Rizzo, "Advanced modelling and preliminary psychophysical experiments for a free-hand haptic device," *Proc. IEEE/RSJ Int. Conf. on Intelligent Robots and Systems*, 1558–1563, 2006.
11. Sgambelluri, N., M. Raugi, R. Rizzo, E.P. Scilingo, and A. Bicchi, "Free hand haptic interfaces based on magnetorheological fluids," *Proceedings of the 14th Symposium on Haptics Interfaces for Virtual Environment and Teleoperator Systems*, Vol. 1, 367–371, 2006.
12. Rossa, C., J. Lozada, and A. Micaelli, "A new hybrid actuator approach for force-feedback devices," *IEEE/RSJ Inter. Conf. on Intelligent Robots and Systems*, 4054–4059, Vilamoura, 2012.
13. Rabinow, J., "The magnetic fluid clutch," *Transactions of the American Institute of Electrical Engineers*, Vol. 67, No. 2, 1308–1315, 1948.
14. Wu, J., X. Jiang, J. Yao, H. Li, and Z. Li, "Design and modeling of a multi-pole and dual-gap magnetorheological brake with individual currents," *Advances in Mechanical Engineering*, Vol. 8, 115, 2016.
15. Forte, P., R. Rizzo, A. Musolino, F. Bucchi, and F. Frendo, "A multi-gap magnetorheological clutch with permanent magnet," *Smart Materials and Structures*, Vol. 24, No. 7, 1–9, 2015.
16. Shiao, Y. and Q. Nguyen, "Development of a multi-pole magnetorheological brake," *Smart Materials and Structures*, Vol. 22, No. 6, 1–13, 2013.
17. Bucchi, F., P. Forte, F. Frendo, A. Musolino, and R. Rizzo, "A fail-safe magnetorheological clutch excited by permanent magnets for the disengagement of automotive auxiliaries," *Journal of Intelligent Material Systems and Structures*, Vol. 25, No. 16, 2102–2114, 2014.
18. Yildirim, G. and S Genc, "Experimental study on heat transfer of the magnetorheological fluids," *Smart Materials and Structures*, Vol. 22, No. 8, 1–8, 2013,
19. Frendo, F., R. Rizzo, A. Musolino, F. Bucchi, and P. Forte, "Magnetic FEM design and experimental validation of an innovative fail-safe magnetorheological clutch excited by permanent magnets," *IEEE Transactions on Energy Conversion*, Vol. 29, No. 3, 628–640, September 2014.
20. Guo, H. T. and W. H. Liao, "A novel multifunctional rotary actuator with magnetorheological fluid," *Smart Materials and Structures*, Vol. 21, No. 6, 1–9, 2012.
21. Johnston, G. L., W. C. Kruckemeyer, and R. E. Longhouse, "Passive Magnetorheological clutch," US Patent, 5848678, 1998.
22. Saito, T. and H. Ikeda, "Development of normally closed type of magnetorheological clutch and its application to safe torque control system of human-collaborative robot," *Journal of Intelligent Material Systems and Structures*, Vol. 18, No. 12, 1181–1185, December 2007.
23. Oh, H.-U., "Characteristics of a magnetorheological fluid isolator obtained by permanent magnet arrangement," *IOP-Smart Mater. Struct.*, Vol. 13, 2004.
24. Wiehe, A. and J. Maas, "Magnetorheological actuators with currentless bias torque for automotive applications," *Journal of Intelligent Material Systems and Structures*, Vol. 21, 1575–1585, 2010.
25. Yang, B., T. Chen, G. Meng, Z. Feng, J. Jiang, S. Zhang, and Q. Zhou, "Design of a safety escape device based on magnetorheological fluid and permanent magnet," *Journal of Intelligent Material Systems and Structures*, Vol. 24, 49–60, 2013.
26. Lai, H. C., R. Rizzo, and A. Musolino, "An electrodynamic/magnetorheological clutch powered by permanent magnets," *IEEE Transactions on Magnetics*, Vol. 53, No. 2, 1–7, February 2017.
27. Tripodi, E., A. Musolino, M. Raugi, and R. Rizzo, "Stabilization of a permanent-magnet system via null-flux coils," *IEEE Trans. on Plasma Science*, Vol. 43, No. 5, 1242–1247, May 2015.
28. Rizzo, R., "An innovative multi-gap clutch based on magneto-rheological fluids and electrodynamic effects: Magnetic design and experimental characterization," *Smart Materials and Structures*, Vol. 26, 1–11, 2017.
29. L. C. Ltd., [www.lord.com/products-and-solutions/magneto-rheological-\(mr\)/mrproducts.xml](http://www.lord.com/products-and-solutions/magneto-rheological-(mr)/mrproducts.xml).
30. Nguyen, Q. H., S. B. Choi, and N. M. Wereley, "Optimal design magnetorheological valves via a finite element method considering control energy and a time constant," *Smart Materials and Structures*, Vol. 17, 25024, 2008.

31. Cardelli, E., "A general hysteresis operator for the modeling of vector fields," *IEEE Transactions on Magnetics*, Vol. 47, No. 8, 20562067, 2011.
32. Cardelli, A. F. E., E. Della Torre, "A general vector hysteresis operator: Extension to the 3-d case," *IEEE Transactions on Magnetics*, Vol. 46, 3990–4000, December 2010.
33. Musolino, A., R. Rizzo, and E. Tripodi, "Tubular linear induction machine as a fast actuator: Analysis and design criteria," *Progress In Electromagnetics Research*, Vol. 132, 603–619, 2012.
34. Aloini, D., E. Crisostomi, M. Raugi, and R. Rizzo, "Optimal power scheduling in a virtual power plant," *IEEE PES International Conference and Exhibition, ISGT*, 1–7, 2011.
35. Tripodi, E., A. Musolino, and R. Rizzo, "The double-sided tubular linear induction motor and its possible use in the electromagnetic aircraft launch system," *IEEE Transactions on Plasma Science*, Vol. 41, No. 5, 1193–1200, May 2013.
36. Raugi, M., A. Musolino, R. Rizzo, and E. Tripodi, "Modeling of the gyroscopic stabilization in a traveling-wave multipole field electromagnetic launcher via an analytical approach," *IEEE Transactions on Plasma Science*, Vol. 43, No. 5, 1236–1241, May 2015.
37. Derbas, H. W., J. M. Williams, A. C. Koenig, and S. D. Pekarek, "A comparison of nodal- and mesh-based magnetic equivalent circuit models," *IEEE Transactions on Energy Conversion*, Vol. 24, No. 2, 388–396, June 2009.
38. Tripodi, E., A. Musolino, R. Rizzo, and M. Raugi, "A new predictor-corrector approach for the numerical integration of coupled electromechanical equations," *Int. J. Numer. Meth. Eng.*, Vol. 105, No. 4, 261–285, 2016.
39. *EFFE v2.00 User Manual*, Bathwick Electrical Design Ltd., 2009.
40. Barmada, S., M. Raugi, M. Tucci, "A multi-objective optimization algorithm based on self-organizing maps applied to wireless power transfer systems," *Int. J. Numer. Mod.: Electronic Networks, Devices and Fields*, Vol 30, No. 3–4, 1–17, 2017.
41. Bartalesi, E., F. Bucchi and R. Squarcini, "Vacuum actuation for axial movement of a magnet in a magnetorheological clutch," *EPO Patent Pending*, 2014.